Acta Mechanica Solida Sinica, Vol. 24, No. 1, February, 2011 ISSN 0894-9166
Published by AMSS Press, Wuhan, China

TRANSIENT RESPONSE OF A BI-LAYERED MULTIFERROIC COMPOSITE PLATE**

Ruifeng Wang[1] **Qingkai Han**[1,2] **Ernian Pan**[1*]

([1] *Computer Modeling and Simulation Group, College of Engineering, University of Akron, Akron, Ohio* 44325-3905*, USA*)

([2] *School of Mechanical Engineering and Automation, Northeastern University, Shenyang* 110004*, China*)

Received 19 May 2010; revision received 20 November 2010

ABSTRACT In this paper, a three-dimensional finite-element formulation for the multiferroic composite is developed and implemented into the commercial software ABAQUS for its transient analysis. First, a special three-dimensional eight-node solid element is designed to handle the multiferroic composite made of elastic, piezoelectric, and piezomagnetic materials. Second, a user-defined subroutine for this newly developed element is implemented into ABAQUS. Finally, the transient responses of a bi-layered multiferroic composite are calculated by using the direct time integration method. Two typical magnetic potential signals, Gauss and Ricker pulses, are applied to the composite with various time durations of excitation. The induced electric field shows that the transient response can be substantially influenced by the input signal, which could be tuned for the strongest electric output.

KEY WORDS transient response, multiferroic, piezoelectric, piezomagnetic, composite, finite element

I. INTRODUCTION

Multiferroic composites have been intensively studied in recent years. Many theoretical[1–8] and numerical[9–12] analyses were carried out under static deformation. While these results are very important in static and/or low-frequency applications and are further essential to understand the coupling features among the elastic, electric and magnetic phases, most real devices operate under dynamic and even transient conditions. For instance, the piezoelectric transducers[13], sensors[14] and actuators[15], and the magnetoelectric effects in multiferroic composites[16,17] are all based on the dynamic motion of the structures in the form of either mechanical vibrations or time-dependent electric/magnetic fields. Furthermore, dynamic analysis is also necessary to unearth the intrinsic characteristics of the multiferroic composites, and the resonance frequency of the multiferroic composite can actually be utilized to enhance the magnetoelectric effect of the structures[18–21], which can be potentially embedded to MEMS devices.

Under transient/dynamic conditions, some theoretical/numerical studies on multiferroic composites were carried out. Hou and Leung[22] and Wang and Ding[23] derived and analyzed the transient response of a multiferroic hollow cylinder under axis-symmetric plane-strain deformation. Daga et al.[24–26] developed a dynamic finite element code for the simulation of multiferroic cylinders and beams. Biju et al.[27] further applied Daga's two-dimensional code[26] to study the response of a sensor bonded to a multiferroic cylindrical shell.

* Corresponding author. E-mail: pan2@uakron.edu

** Project partially supported by the National Natural Science Foundation of China (No. 50775028).

While the previous static and transient/dynamic analyses are important to our understanding of the multiferroic composites, they are limited to simple geometries under ideal conditions. Therefore, it is necessary to develop a numerical model that is more flexible and can be applied to the actual device analysis. As the first step towards this goal, we extend, in this article, our previously designed three-dimensional (3D) finite elements (FEs) for multiferroic composites[12] from static to dynamic analysis. The new FEs are coded and implemented into the commercial software ABAQUS[28]. The direct integration method, namely the Hilber-Hughes-Taylor method[29], is utilized to carry out the time-domain integration. Two kinds of transient magnetic potential excitations, Gauss and Ricker pulses, are applied as input to a bi-layered multiferroic composite made of a piezoelectric (PE) and piezomagnetic (PM) layer. The induced transient electric responses are calculated and analyzed along with the natural frequencies of the composite.

II. THREE-DIMENSIONAL FE FORMULATION

We discrete the multiferroic composite plate with three-dimensional eight-node solid elements where there are five degrees of freedom (DOFs) at each node. The extended displacement vector $\boldsymbol{u}_i$ at node i is defined as

$$\boldsymbol{u}_i = \left\{ u \quad v \quad w \quad \phi \quad \psi \right\}_i^{\mathrm{T}} \tag{1}$$

where u, v, and w are the elastic displacements along the x-, y- and z-directions respectively, and ϕ and ψ are the electric and magnetic potentials at node i. Then the global displacement vector of the entire plate discretized with a total of n nodes is expressed as

$$\boldsymbol{u} = \left\{ \boldsymbol{u}_1 \quad \boldsymbol{u}_2 \quad \cdots \quad \boldsymbol{u}_i \quad \cdots \quad \boldsymbol{u}_n \right\}^{\mathrm{T}} \tag{2}$$

Similar to the purely elastic case, the dynamical equations of the nodal motions for the multiferroic composite plate can be written as

$$\boldsymbol{M}\ddot{\boldsymbol{u}}(t) + \boldsymbol{\Lambda}\dot{\boldsymbol{u}}(t) + \boldsymbol{K}\boldsymbol{u}(t) = \boldsymbol{P}(t) \tag{3}$$

where $\boldsymbol{\Lambda}$ is the global damping matrix to be discussed later on; $\boldsymbol{P}(t)$ is the global load vector as a function of time t; $\boldsymbol{M}$ and $\boldsymbol{K}$ are the global mass and stiffness matrices, respectively, assembled from their corresponding element mass matrix $\boldsymbol{M}^e$ and stiffness matrix $\boldsymbol{K}^e$. By letting $\boldsymbol{N}$ be the shape function matrix of the eight-node element, the extended element mass and stiffness matrices can be expressed as the following volumetric integration over the element volume V_e as

$$\boldsymbol{M}^e = \int_{V_e} \boldsymbol{N}^{\mathrm{T}} \boldsymbol{\rho} \boldsymbol{N} \mathrm{d}V, \quad \boldsymbol{K}^e = \int_{V_e} \boldsymbol{B}^{\mathrm{T}} \boldsymbol{D} \boldsymbol{B} \mathrm{d}V \tag{4}$$

where $\boldsymbol{\rho}$ and $\boldsymbol{D}$ are the extended material density and material stiffness matrices, and $\boldsymbol{B}$ is the extended strain-gradient matrix to be defined later on. The extended density matrix $\boldsymbol{\rho}$ is

$$\boldsymbol{\rho} = \begin{bmatrix} \rho & & & & \\ & \rho & & 0 & \\ & & \rho & & \\ & 0 & & 0 & \\ & & & & 0 \end{bmatrix} \tag{5}$$

with ρ being the density of the material within the element.

For an anisotropic multiferroic material, the extended constitutive equation can be expressed as

$$\begin{Bmatrix} \boldsymbol{\sigma} \\ \boldsymbol{d} \\ \boldsymbol{b} \end{Bmatrix} = \boldsymbol{D} \begin{Bmatrix} \boldsymbol{\gamma} \\ -\boldsymbol{E} \\ -\boldsymbol{H} \end{Bmatrix} \tag{6}$$

with the extended material stiffness matrix $\boldsymbol{D}$ being defined as

$$\boldsymbol{D} = \begin{bmatrix} \boldsymbol{C} & \boldsymbol{e} & \boldsymbol{q} \\ \boldsymbol{e}^{\mathrm{T}} & -\boldsymbol{\varepsilon} & -\boldsymbol{\alpha} \\ \boldsymbol{q}^{\mathrm{T}} & -\boldsymbol{\alpha}^{\mathrm{T}} & -\boldsymbol{\mu} \end{bmatrix} \tag{7}$$

In Eq.(6), $\boldsymbol{\sigma}$, $\boldsymbol{d}$ and $\boldsymbol{b}$ are the vectors of the elastic stress, electric displacement and magnetic induction; $\boldsymbol{\gamma}$, $\boldsymbol{E}$ and $\boldsymbol{H}$ are the vectors of the elastic strain, electric field and magnetic field. In the extended material stiffness matrix expression (7), $\boldsymbol{C}$, $\boldsymbol{e}$, $\boldsymbol{q}$, $\boldsymbol{\varepsilon}$, $\boldsymbol{\alpha}$, $\boldsymbol{\mu}$ are the matrices of the elastic stiffness, piezoelectric, piezomagnetic, electric permittivity, magnetoelectric coupling, and magnetic permeability coefficients, respectively. For a layered multiferroic composite made of PE and PM layers, the extended material stiffness matrix Eq.(7) is, respectively, simplified to

$$\boldsymbol{D}_{\mathrm{PE}} = \begin{bmatrix} \boldsymbol{C} & \boldsymbol{e} & \boldsymbol{0} \\ \boldsymbol{e}^{\mathrm{T}} & -\boldsymbol{\varepsilon} & \boldsymbol{0} \\ \boldsymbol{0} & \boldsymbol{0} & -\boldsymbol{\mu} \end{bmatrix}, \quad \boldsymbol{D}_{\mathrm{PM}} = \begin{bmatrix} \boldsymbol{C} & \boldsymbol{0} & \boldsymbol{q} \\ \boldsymbol{0} & -\boldsymbol{\varepsilon} & \boldsymbol{0} \\ \boldsymbol{q}^{\mathrm{T}} & \boldsymbol{0} & -\boldsymbol{\mu} \end{bmatrix} \tag{8}$$

The extended element strain matrix $\boldsymbol{B}$ is derived using the following extended deformation and strain relations

$$\begin{aligned} \boldsymbol{\gamma} &= \left\{ \frac{\partial u}{\partial x} \quad \frac{\partial v}{\partial y} \quad \frac{\partial w}{\partial z} \quad \frac{\partial v}{\partial z} + \frac{\partial w}{\partial y} \quad \frac{\partial u}{\partial z} + \frac{\partial w}{\partial x} \quad \frac{\partial u}{\partial y} + \frac{\partial v}{\partial x} \right\}^{\mathrm{T}} \\ \boldsymbol{E} &= -\left\{ \frac{\partial \phi}{\partial x} \quad \frac{\partial \phi}{\partial y} \quad \frac{\partial \phi}{\partial z} \right\}^{\mathrm{T}}, \quad \boldsymbol{H} = -\left\{ \frac{\partial \psi}{\partial x} \quad \frac{\partial \psi}{\partial y} \quad \frac{\partial \psi}{\partial z} \right\}^{\mathrm{T}} \end{aligned} \tag{9}$$

Expressing the matrix $\boldsymbol{B}$ as

$$\boldsymbol{B} = \begin{bmatrix} \boldsymbol{B}_1 & \boldsymbol{B}_2 & \boldsymbol{B}_3 & \boldsymbol{B}_4 & \boldsymbol{B}_5 & \boldsymbol{B}_6 & \boldsymbol{B}_7 & \boldsymbol{B}_8 \end{bmatrix} \tag{10}$$

we find that, in terms of the shape functions N_i, its node associated components are $(i = 1, 8)$

$$\boldsymbol{B}_i = \begin{bmatrix} \frac{\partial N_i}{\partial x} & 0 & 0 & 0 & \frac{\partial N_i}{\partial z} & \frac{\partial N_i}{\partial y} & 0 & 0 & 0 & 0 & 0 & 0 \\ 0 & \frac{\partial N_i}{\partial y} & 0 & \frac{\partial N_i}{\partial z} & 0 & \frac{\partial N_i}{\partial x} & 0 & 0 & 0 & 0 & 0 & 0 \\ 0 & 0 & \frac{\partial N_i}{\partial z} & \frac{\partial N_i}{\partial y} & \frac{\partial N_i}{\partial x} & 0 & 0 & 0 & 0 & 0 & 0 & 0 \\ 0 & 0 & 0 & 0 & 0 & 0 & \frac{\partial N_i}{\partial x} & \frac{\partial N_i}{\partial y} & \frac{\partial N_i}{\partial z} & 0 & 0 & 0 \\ 0 & 0 & 0 & 0 & 0 & 0 & 0 & 0 & 0 & \frac{\partial N_i}{\partial x} & \frac{\partial N_i}{\partial y} & \frac{\partial N_i}{\partial z} \end{bmatrix}^{\mathrm{T}} \tag{11}$$

If we assume that the elements are isoparametric, the space coordinates as well as all physical quantities can be approximated by the same set of shape functions. For the 8-node brick element, the shape function at node i in the intrinsic coordinates (ξ,η,ζ) can be expressed as

$$N_i = \frac{1}{8}(1 + \xi_i \xi)(1 + \eta_i \eta)(1 + \zeta_i \zeta) \quad (i = 1, \ldots, 8) \tag{12}$$

Thus, by applying the Gauss quadrature to the volumetric integration involved, the extended element mass and stiffness matrices can be evaluated element by element. By further assembling these elements together, the global matrices $\boldsymbol{M}$ and $\boldsymbol{K}$of the composite plate can be obtained.

Considering a proportional damping in the plate, the global damping matrix $\boldsymbol{\Lambda}$ in Eq.(3) can be expressed as a linear combination of the global matrices $\boldsymbol{M}$ and $\boldsymbol{K}$ in the form

$$\boldsymbol{\Lambda} = \alpha \boldsymbol{M} + \beta \boldsymbol{K} \tag{13}$$

where α and β are the Rayleigh damping coefficients depending on the material and structure of the problem, respectively. Their values will be discussed and given in numerical examples later on.

Therefore, all the coefficient matrices are determined in the dynamic equation (3). Then we can input our user-defined subroutines based on the above FE formula into the commercial software ABAQUS to solve both the dynamic and transient responses of the composite plate. In particular, the Lanczos method is applied to extract the eigenfrequencies and the implicit Hilber-Hughes-Taylor operator is employed for the time-domain integration in transient analysis.

III. NATURAL FREQUENCIES AND TRANSIENT RESPONSES

Shown in Fig.1 is a bi-layered multiferroic composite plate. Its top layer is PE material PZT-5A and bottom layer is PM material $CoFe_2O_4$. The two layers are assumed to be well bonded together. In other words, the displacement and traction vectors, the z-components of the electric displacement and magnetic induction are all continuous along the interface of the two layers. The polarizations of both materials are along the z-direction, with their material properties being listed in Table 1. The geometry of the bi-layered plate is: $L_x = 16$ mm, $L_y = 6.4$ mm, $t_e = t_m = 1$ mm. The composite plate is discretized with a total of 10000 brick elements by using our newly designed solid multiferroic elements. This discretization corresponds to the mesh grids $n_x = 50$, $n_y = 20$ and $n_z = 5$ for both PE and PM layers. Numerical results presented below are based on this mesh size, with a relative error less than 5%. For each time step, it requires roughly 140 s to run the program on a Dell desktop computer with 2.4 GHz CPU and 3 GB memory. We further mention that for the corresponding piezoelectric and purely elastic cases, our numerical solutions reduce exactly to those from ANSYS.

The mechanical translation and rotation DOFs (i.e., the rigid-body motions) of the composite plate are constrained at the three corners on the bottom surface: For the point with $(x, y, z) = (0, 0, -t_m)$ (Fig.1) the mechanical boundary condition (MBC) is $u = v = w = 0$; for the point with $(x, y, z) = (L_x, 0, -t_m)$, the MBC is $v = w = 0$; for the point with $(x, y, z) = (0, L_y, -t_m)$, the MBC is $w = 0$. The magnetic potential at the bottom surface is set to zero and a dynamic magnetic potential is applied at the interface of the bi-layered plate. Thus a dynamic magnetic field along the z-direction is produced between the two surfaces of the PM layer. A dynamic electric field will be induced along the z-direction in the PE layer. By assuming that the electric potential at the interface is zero, a dynamic voltage response can be calculated on the top surface of the PE layer.

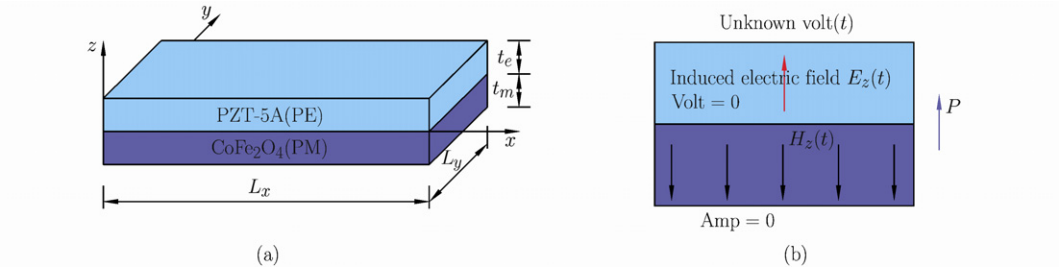

Fig. 1. A bi-layered PE/PM multiferroic composite plate: geometry in (a), the electric and magnetic boundary conditions with the applied dynamic magnetic field H_z(t) in (b). This magnetic field is calculated from the applied magnetic potentials on the two surfaces of the PM layer.

Before carrying out the transient response of the bi-layered composite, we first investigate its natural frequencies. By employing the ABAQUS Lanczos eigensolver, the characteristic equations of the composite plate are extracted for the natural frequencies. The first 7 natural frequencies are listed in Table 2. These natural frequencies will be used to determine the Rayleigh damping coefficients α and β in Eq.(13). It can be seen that, for the given geometry and material properties of the composite, its natural frequencies are very low, with its fundamental one being 7810 Hz.

In order to simulate the transient response of the multiferroic plate, the system damping needs to be considered. Similar to the analysis of elastic and piezoelectric systems[30], we adopt the Rayleigh damping for the current structure with the damping matrix being expressed as a linear combination of the mass and stiffness matrices as in Eq.(13). Furthermore, the Rayleigh damping coefficients α and β in Eq.(13) are determined approximately in the given range of two different natural frequencies ω_1 and ω_2 by[31]

$$\begin{Bmatrix} \alpha \\ \beta \end{Bmatrix} = \begin{bmatrix} \dfrac{1}{2\omega_1} & \dfrac{\omega_1}{2} \\ \dfrac{1}{2\omega_2} & \dfrac{\omega_2}{2} \end{bmatrix}^{-1} \begin{Bmatrix} \xi_1 \\ \xi_2 \end{Bmatrix} \tag{14}$$

Table 1. **Material properties of PZT-5A (PZT) and $CoFe_2O_4$(CFO)[12](C_{ij}: elastic constants in GPa; e_{ij}: piezoelectric coefficients in N/(Vm); q_{ij}: piezomagnetic coefficients in N/(Am); ε_{ij}: permittivity coefficients in 10^{-8} C/(Vm); μ_{ij}: permeability coefficients in 10^{-6} Wb/(Am); and ρ: density in 10^3 kgm^{-3})**

	PZT	CFO		PZT	CFO
C_{11}	99.201	286	e_{51}	12.332	0
C_{12}	54.016	173	q_{13}	0	580.3
C_{13}	50.778	170.5	q_{23}	0	580.3
C_{22}	99.201	286	q_{33}	0	699.7
C_{23}	50.778	170.5	q_{42}	0	550
C_{33}	86.856	269.5	q_{51}	0	550
C_{44}	21.1	45.3	ε_{11}	1.53	–
C_{55}	21.1	45.3	ε_{22}	1.53	–
C_{66}	22.593	56.5	ε_{33}	1.5	–
e_{13}	−7.209	0	μ_{11}	–	590
e_{23}	−7.209	0	μ_{22}	–	590
e_{33}	15.118	0	μ_{33}	–	157
e_{42}	12.332	0	ρ	5.3	5.7

Table 2. **The first seven natural frequencies of the multiferroic composite plate**

Mode No.	1	2	3	4	5	6	7
Natural frequency f_i (Hz)	7810	9934	16183	19018	24617	31160	48238

where, ξ_1 and ξ_2 are the corresponding modal damping ratios. In this study, they are assumed to be 0.05 and 0.03, respectively.

As numerical examples, the transient response of the multiferroic composite under a magnetic field excitation is analyzed. As described in the previous section, the magnetic potential at the bottom surface is assumed to be zero, and a short-term magnetic potential ψ(or signal) is applied at the interface of the bi-layered plate. We consider two kinds of input magnetic potential signals given by

$$\psi_G(t) = A_0 \mathrm{e}^{-(10ct-t_0)^2/2} \tag{15}$$

$$\psi_R(t) = A_0[1-(10ct-t_0)^2]\mathrm{e}^{-(10ct-t_0)^2/2} \tag{16}$$

where, A_0, t_0 and c are the impulse function parameters. While Eq.(15) is the Gauss pulse (the signal function is a Gauss function of time), Eq.(16) is the Ricker pulse.

Both excitations are typical input impulse functions used in transient analysis. They are short-term pulse with time duration less than millisecond in our examples. By changing the parameters t_0 and c, various shapes of input signals can be obtained. For instance, Figs.2(a) and 2(b) show, respectively,

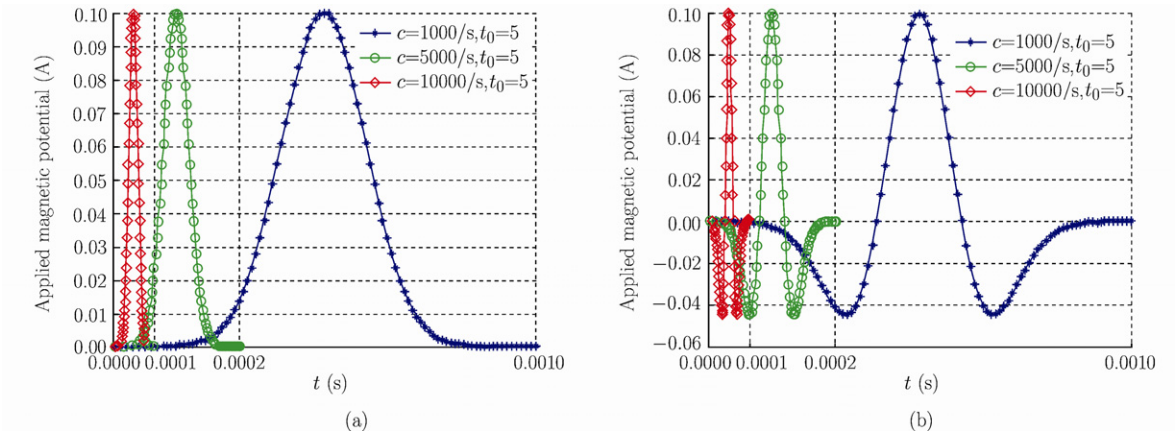

Fig. 2. Input magnetic potentials as Gauss (a) and Ricker (b) functions of time applied on the interface of the bi-layered plate for three different time durations. The horizontal time axis is not equally scaled.

the Gauss and Ricker input signals considered in this study. For both signal functions, we vary c as 1000/s, 5000/s and 10000/s while fixing t_0 at 5. It is clearly observed from these figures that a large c corresponds to a short-time excitation. Note that the time scale for different signals in Figs.2(a) and 2(b) is not uniform. The peak amplitude of the magnetic potential signal in Eqs.(15) and (16) is chosen as $A_0 = 0.1$ A in order to restrain our study in the linear range where the magnetic permeability coefficients can be assumed to be constant[5, 12].

By applying the above magnetic potentials to the interface of the bi-layered plate while fixing the magnetic potential on the bottom surface of the PM layer at zero (Fig.1), the electric potential on the top surface of the PE layer can be solved. Note that at different nodes on the top surface, the induced voltage response will be different. Figures 3(a), 3(b) and 3(c) show the induced electric potential at the center of the PE surface, respectively, for parameter $c = 1000$/s, 5000/s and 10000/s. The following features are observed from these figures: (1) For $c = 1000$/s, the induced time-dependent voltage curves are similar in shape to their corresponding input magnetic Gauss and Ricker pulses, and these responses immediately vanish after the excitation is removed. For $c = 5000$/s and $c = 10000$/s, the induced voltage-time curves have obviously different shapes to the input magnetic pulse, and the induced voltage curve still oscillate away from zero after the input signal is removed. (2) With increasing c ($c = 1000$/s, 5000/s and 10000/s), the peak magnitude of the induced voltage increases. This is expected since excitations with different time durations, even though their amplitudes are the same, would always induce different responses in the structure. (3) It is further noted that even for a relatively slow impulse ($c = 1000$/s), the induced voltage possesses a peak magnitude slightly higher than the corresponding static case[12]. (4) For both $c = 5000$/s and $c = 10000$/s, the voltage response of the Ricker pulse has a higher amplitude than that

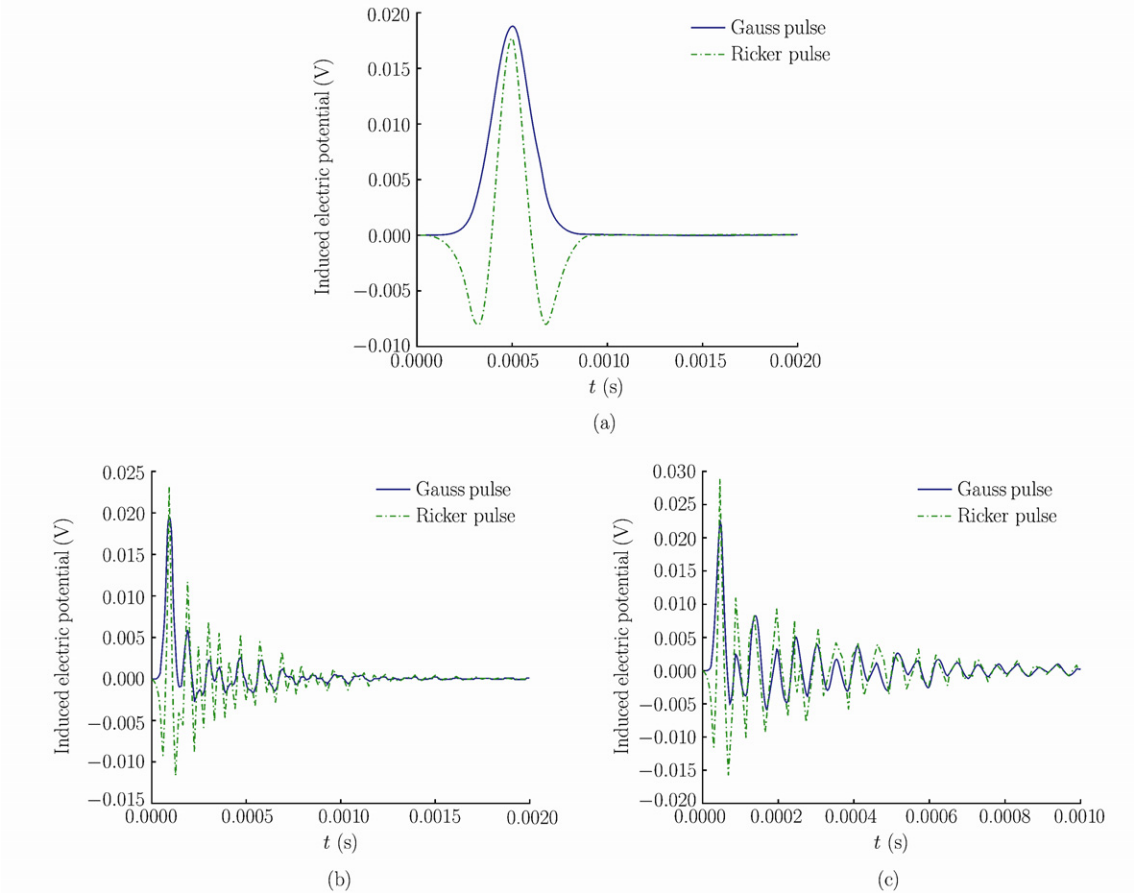

Fig. 3. Transient voltage response at the center on the top surface of the PE layer induced by the dynamic magnetic field in both Gauss and Ricker variations applied to the PM layer with a time duration $t = 0.001$ s (a), $t = 0.0002$ s (b) and $t = 0.0001$ s (c), respectively (i.e., corresponds to $c = 1000$/s, 5000/s, and 10000/s, respectively).

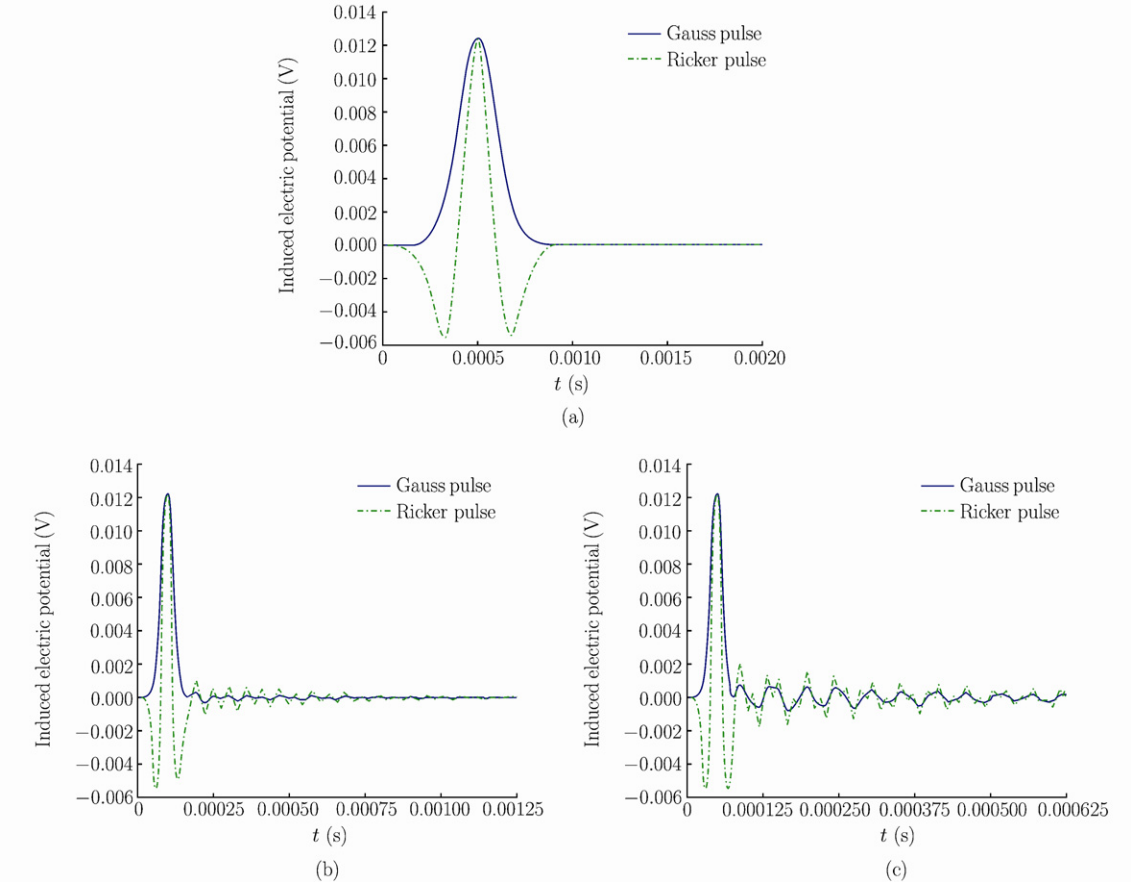

Fig. 4. Transient voltage response at the corner $(x, y, z) = (L_x, L_y, t_e)$ on the top surface of the PE layer induced by the dynamic magnetic field in both Gauss and Ricker variations applied to the PM layer with a time duration $t = 0.001$ s (a), $t = 0.0002$ s (b) and $t = 0.0001$ s (c), respectively (i.e., corresponds to $c = 1000/\text{s}$, $5000/\text{s}$, and $10000/\text{s}$, respectively).

of the Gauss pulse. These features could be very useful for optimal tuning of the electric output of the multiferroic composite.

Figures 4(a), 4(b) and 4(c) show the induced electric potential at one of the corners $(x, y, z) = (L_x, L_y, t_e)$ in Fig.1 on the surface of the PE layer, respectively, for $c = 1000/\text{s}$, $5000/\text{s}$ and $10000/\text{s}$. Compared to Fig.3, it is clear that the voltage response at the corner is very similar to that at the center of the surface of the PE layer. However, at the corner, the voltage magnitude is much smaller, a feature similar to the corresponding static case[12]. It is also noted that for $c = 5000/\text{s}$ and $c = 10000/\text{s}$, the time duration of the surface electric response at the corner is much shorter than that at the center. Furthermore, in contrast to the response at the center where a different c corresponds to a different amplitude, the peak values at the corner for the three different c are nearly the same.

IV. CONCLUSIONS

We developed a three-dimensional finite-element formulation for the multiferroic composite and implemented it into the commercial software ABAQUS for transient analyses of the composite. Numerical examples are carried out for two typical magnetic potential signals, Gauss and Ricker pulses, with various time durations of excitation, applied to a bi-layered multiferroic composite. It is found that the induced electric field could be substantially altered by the input signal, an interesting feature which could serve as a new avenue for optimal tuning of the electric output.

References

[1] Nan,C.W., Magnetoelectric effect in composites of piezoelectric and piezomagnetic phases. *Physical Review B*, 1994, 50: 6082-6088.

[2] Wu,T.L. and Huang,J.H., Closed-form solutions for the magnetoelectric coupling coefficients in fibrous composites with piezoelectric and piezomagnetic phases. *International Journal of Solids and Structures*, 2000, 37: 2981-3009.
[3] Pan,E., Exact solution for simply supported and multilayered magneto-electro-elastic plate. *Journal of Applied Mechanics*, 2001, 68: 608-618.
[4] Chen,W.Q. and Lee,K.Y., Alternative state space formulations for magnetoelectric thermoelasticity with transverse isotropy and the application to bending analysis of nonhomogeneous plates. *International Journal of Solids and Structures*, 2003, 40: 5689-5705.
[5] Dong,S.X., Li,J.F. and Viehland,D., Longitudinal and transverse magnetoelectric voltage coefficients of magnetostrictive/piezoelectric laminate composite: theory. *IEEE Transactions on Ultrasonics, Ferroelectrics and Frequency Control*, 2003, 50: 1253-1261.
[6] Pan,E., Wang,X. and Wang,R., Enhancement of magnetoelectric effect in multiferroic fibrous nanocomposites via size-dependent material properties. *Applied Physics Letter*, 2009, 95: 181904.
[7] Zhang,C.L., Yang,J.S. and Chen,W.Q., Magnetoelectric effects in multiferroic bilayers for coupled flexure and extensions. *Journal of Intelligent Material Systems and Structures*, 2010, 21: 851-855.
[8] Wang,R., Han,Q.K. and Pan,E., An analytical solution for a multilayered magneto-electro-elastic circular plate under simply supported lateral boundary conditions. *Smart Materials and Structures*, 2010, 19: 065025.
[9] Lage,R.G., Soares,C.M.M., Soares,C.A.M. and Reddy.J.N., Layerwise partial mixed finite element analysis of magneto-electro-elastic plates. *Computers and Structrues*, 2004, 82: 1293-1301.
[10] Liu,G., Nan,C.W., Cai,N. and Lin,Y.H., Calculations of giant magnetoelectric effect in multiferroic composites of rare-earth-iron alloys and PZT by finite element method. *International Journal of Solids and Structures*, 2004, 41: 4423-4434.
[11] Bhangale,R.K. and Ganesan,N., Static analysis of simply supported functionally graded and layered magneto-electro-elastic plates. *International Journal of Solids and Structure*, 2006, 43: 3230-3253.
[12] Pan,E. and Wang,R., Effects of geometric size and mechanical boundary conditions on magnetoelectric coupling in multiferroic composites. *Journal of Physics D: Applied Physics*, 2009, 42: 245503.
[13] Ward,M. and Buttry,D., In situ interfacial mass detection with piezoelectric transducers. *Science*, 1990, 245: 1000-1007.
[14] Sirohi,J., Fundamental understanding of piezoelectric strain sensors. *Journal of Intelligent Material Systems and Structures*, 2000, 4: 246-257.
[15] Crawley,E.F. and Luis,J., Use of piezoelectric actuators as elements of intelligent structures. *AIAA Journal*, 1987, 25: 1373-1385.
[16] Kumar,M., Srinivas,A., Suryanarayana,S., Kumar,G. and Bhimasankaram,T., An experimental setup for dynamic measurement of magnetoelectric effect. *Bulletin of Materials Science*, 1998, 21: 251-255.
[17] Srinivasan,G., Vreugd,C., Laletin,V.M., Paddubnaya,N., Bichurin,M.I., Petrov,V.M. and Filippov,D.A., Resonant magnetoelectric coupling in trilayers of ferromagnetic alloys and piezoelectric lead zirconate titanate: The influence of bias magnetic field. *Physical Review B*, 2005, 71: 184423.
[18] Bichurin,M.I., Filippov,D.A., Petrov,V.M., Laletsin,V.M., Paddubnaya,N. and Srinivasan,G., Resonance magnetoelectric effects in layered magnetostrictive-piezoelectric composites. *Physical Review B*, 2003, 68: 132408.
[19] Filippov,D.A., Bichurin,M.I., Petrov,V.M., Laletin,V. M., Poddubnaya,N. and Srinivasan,G., Giant magnetoelectric effect in composite materials in the region of electromechanical resonance. *Technical Physics Letters*, 2004, 30: 15-20.
[20] Gheevarughese,V., Laletsin,U., Petrov,V.M., Srinivasan,G. and Fedotov,N.A., Low-frequency and resonance magnetoelectric effects in lead zirconate titanate and single-crystal nickel zinc ferrite bilayers. *Journal of Materials Research*, 2007, 22: 2130-2135.
[21] Wang,H.M., Pan,E. and Chen,W.Q., Enhancing magnetoelectric effect via the curvature of composite cylinder. *Journal of Applied Physics*, 2010, 107: 093514.
[22] Hou,P. and Leung,A.Y.T., The transient responses of magneto-electro-elastic hollow cylinders. *Smart Materials and Structures*, 2004, 13: 762-776.
[23] Wang,H.M. and Ding,H.J., Transient responses of a special non-homogeneous magneto-electro-elastic hollow cylinder for a fully coupled axisymmetric plane strain problem. *Acta Mechanica*, 2006, 184: 137-157.
[24] Daga,A., Ganesan,N. and Shankar,K., Comparative studies of the transient Response for PECP, MSCP, Barium Titanate, magneto-electro-elastic finite cylindrical Shell under constant internal pressure using finite element method. *Finite Element Analysis and Design*, 2008a, 44: 89-104.
[25] Daga,A., Ganesan,N. and Shankar,K., Transient response of magneto-electro-elastic simply supported cylinder using finite element. *Journal of Mechanics of Materials and Structures*, 2008b, 3: 375-389.
[26] Daga,A., Ganesan,N. and Shankar,K., Transient dynamic response of cantilever magneto-electro-elastic beam using finite elements. *International Journal for Computational Methods in Engineering Science and Mechanics*, 2009, 10: 173-185.

[27] Biju,B., Ganesan,N. and Shankar,K., The transient dynamic response of multiphase magneto-electro-elastic sensors bonded to a shell structure. *Journal of Materials: Design and Applications*, 2010, 224 (In Press).
[28] ABAQUS Version 6.7 Documentation, http: //coel3.ecgf.uakron.edu: 2080/v6.7 *Dassault Systèmes Simulia.*
[29] Hilber,H.M. and Hughes,T.J.R., Collocation, dissipation and 'overshoot' for time integration schemes in structural dynamics. *Earthquake Engineering and Structural Dynamics*, 1978, 6: 99-117.
[30] Chandrashekhara,K. and Agarwal,A.N., Active vibration control of laminated composite plates using piezoelectric devices: A finite element approach. *Journal of Intelligent Material Systems and Structures*, 1993, 4: 496-508.
[31] Thomson,W.T. and Dahleh,M.D., Theory of Vibration with Applications, 5th edn. New Jersey: Prentice Hall, 1993.